

Atomic-scale imaging and the effect of yttrium on the fracture toughness of silicon carbide ceramics

A.M. Kueck^{a,b}, Q.M. Ramasse^c, L.C. De Jonghe^{a,b}, R.O. Ritchie^{a,b,*}

^a Department of Materials Science & Engineering, University of California, Berkeley, CA 94720, USA

^b Materials Sciences Division, Lawrence Berkeley National Laboratory, Berkeley, CA 94720, USA

^c National Center for Electron Microscopy, Lawrence Berkeley National Laboratory, Berkeley, CA 94720, USA

Received 6 January 2010; accepted 22 January 2010

Available online 17 February 2010

Abstract

In SiC sintered with Al, B and C additions (ABC–SiC), the presence of Y in the Al–Si–O–C grain-boundary phase leads to less frequent crack deflection and lower toughness. When Y is absent from the grain-boundary phase and remains in the triple pockets, crack deflection is restored, and higher toughness results from grain-bridging mechanisms. The observations are consistent with elastic modulus changes in the intergranular phase, which depend on their yttria and silica content, and indicate that these can play an important role in determining crack deflection. While high-toughness ceramics such as ABC–SiC and Si₃N₄ rely on sintering additives forming crack-deflecting intergranular films, the present case is a striking example where the presence of a segregant in the grain boundary promotes transgranular fracture by raising the modulus of the nanoscale intergranular grain-boundary film.

© 2010 Acta Materialia Inc. Published by Elsevier Ltd. All rights reserved.

Keywords: Ceramics; Silicon carbide; Yttrium dopants; Fracture toughness

1. Introduction

Rare-earth (RE) additives are commonly used as sintering aids in the processing of silicon carbide and silicon nitride structural ceramics. Much work has focused on the role of these additives, in particular on ionic size and its influence on mechanical properties such as strength, toughness and creep resistance. It is widely reported that the fracture toughness of SiC and Si₃N₄ increases with increasing RE ionic radius of the additives [1–3], an effect which the present authors believe can be understood by the change in the stiffness of the grain-boundary phase due to the presence of the RE ions [4]. However, with additions of yttrium, which is of intermediate ionic size, the mechanism is less clear. Studies show that SiC and Si₃N₄ with Y additives can fail by transgranular fracture [1], intergranular fracture [5–7] or both

[2,8,9]. The nature of the fracture mode is critical to the mechanical properties of the ceramic. Intergranular fracture can lead to crack-tip shielding by (interlocking) grain bridging,¹ which promotes rising resistance-curve (R-curve) behavior and high fracture toughness (approaching, or even exceeding, 10 MPa m^{1/2}); with transgranular (cleavage) fracture, there is no such crack bridging or rising R-curves, and the fracture toughness is invariably low (typically ~2–3 MPa m^{1/2}). Low toughness and the lack of a rising R-curve causes low damage tolerance and can also lead to lower strength [11]. Previous results with Y-containing SiC suggest that Y itself plays a critical role in determining the fracture mode, and hence the fracture toughness, of the material.

¹ Grain bridging is an extrinsic toughening mechanism [10] which enhances the toughness by operating in the wake of the crack tip to “shield” the crack tip from the full (applied) driving force. The crack bridges then carry loads that would otherwise be used to propagate the crack further, thereby increasing the measured fracture toughness.

* Corresponding author. Address: Department of Materials Science & Engineering, University of California, Berkeley, CA 94720, USA. Tel.: +1 510 486 5798; fax: +1 510 643 7294.

E-mail address: RORitchie@lbl.gov (R.O. Ritchie).

Difficulties in imaging yttrium with *Z*-contrast scanning transmission electron microscopy (STEM) or collecting yttrium electron energy loss spectroscopy (EELS) signals have hindered the development of a reliable means of characterizing the grain-boundary phase with high (i.e., atomic) spatial resolution [8,12,13]. While it is generally agreed that the presence of specific sintering additives governs the nature of this phase, which in turn dictates whether fracture occurs by high-toughness intergranular or low-toughness transgranular cracking, the exact cause of this transition for Y-containing silicon carbide (and nitride) has not been determined.

Here, atomic-resolution transmission electron microscopy (TEM) is used to examine two similar compositions of yttrium-doped silicon carbides which exhibit either intergranular or transgranular fracture. It is demonstrated that it is the atomic-scale presence (or absence) of Y within the high-silica grain-boundary phase that directly correlates with the marked differences in macro-scale fracture toughness of these ceramics.

2. Experimental procedures

2.1. Sample processing

SiC powders were prepared with 0.5 or 0.7 at.% Y; acetate salts of yttrium were dissolved in methanol and added to sub-micrometer β -SiC powder (Betarundum, grade Ultrafine, IBI-DEN, Japan), with a mean particle size of 0.27 μm , 3 wt.% Al metal, 0.6 wt.% B and 6 wt.% carbon source. The Al powder (H-3, Valimet, Stockton, CA) had an average size of 3 μm ; the boron powder (Alfa Aesar) had a particle size of <5 μm . The carbon was added as polyvinylbutyral, which yielded $\sim 33\%$ C by weight upon pyrolysis. The powder slurry was ultrasonically agitated, stir-dried, and sieved through a 200-mesh screen. Discs of the mixed powders 38 mm in diameter were pre-formed at ambient temperature in a steel die, before being hot-pressed in a graphite die. Hot pressing was conducted at 1900 °C with 50 MPa applied pressure under flowing argon at 1 atm, with heating and cooling rates of 10 °C min^{-1} . Hot-pressed rounds were ground to remove ~ 0.5 mm from each surface. The resulting 0.5 at.% Y- and 0.7 at.% Y-containing SiC ceramics are referred to throughout this paper as Y0.5 and Y0.7, respectively.

2.2. Fracture testing

To examine the fracture properties, Vickers micro-indentations with a 10 kg load on a polished surface of the ceramics were used to generate cracks, which were then examined in the scanning electron microscope (JEOL JSM-6340F SEM) to discern the overall crack path. At least 12 cracks in each specimen were observed in the microscope to characterize the fracture behavior. Additionally, indentation toughness was measured from these indents. Ten indents and ~ 30 cracks were used for each measurement.

The fracture toughness was further estimated using the controlled-flaw method, where indentations on the tensile

surface of beams provide the initial flaws which lead to fracture. Five unindented beams were tested in four-point bend, inner span 10 mm and outer span 25 mm, with a displacement rate of 0.05 mm min^{-1} , along with four beams with indentations. Three indentations were placed within the inner span on the tensile surface, spaced 2 mm apart. Critical flaw sizes were estimated to be ~ 100 μm , based on the original crack length and confirmed by observation of the post-mortem fracture surfaces. Fracture toughness values were calculated from the strength of the indented beams based on the method of Cao et al. [14,15].

As SiC is intended to be a high-temperature material, further fracture tests were carried out at 1200 °C. Crack-growth resistance curves (R-curves) were generated using compact-tension DC(T) specimens. Cracks were initiated at room temperature from razor micronotches with a root radius of ~ 10 μm and grown to ~ 5 – 10 μm before high temperature testing. Crack lengths were measured in situ by the DC potential-drop method described in Refs. [16,17], and corrected by observing the final crack size after test completion. Tests were conducted in a graphite resistance furnace under flowing Ar at ~ 1 atm at a displacement rate of 0.05 mm min^{-1} .

2.3. TEM and spectroscopy

To gain information on the crack path at atomistic dimensions, specifically on how cracks interact with the grain boundaries and the boundary phases, a new technique of indenting TEM foils was used [4]. The method is based on the procedure of Sun et al. [18] to estimate the interfacial toughness of glassy phases in ceramics from the elastic mismatch across the interface. TEM foils were prepared from material at least 1 mm from the edge of the specimen. Stable cracks were produced to allow observation the composition of the crack faces. Cracks in the TEM foils were introduced via indentation, which was performed before final milling on a 200- μm -thick section; an array of 10×10 micro-indents (50 g load with a cube-corner indenter) was produced on a polished surface. Mechanical thinning and ion milling proceeded from the opposite side to preserve the cracks. Their propagation paths as they impinged on grain boundaries were then specifically examined.

A Philips CM200/FEG transmission electron microscope with energy dispersive spectroscopy (EDS), operating in the STEM mode with a 1-nm spot size, was employed to analyze the chemistry of the fracture surfaces. High-resolution high-angle annular dark field (HAADF or *Z*-contrast) images of uncracked grain boundaries were also obtained using an aberration-corrected VG HB501 STEM with a spot size of 0.1 nm [19].

3. Results

The two SiC ceramics studied had different Y contents, denoted Y0.5 and Y0.7 for Y doping levels of 0.5 and 0.7 at.%, respectively, but otherwise had similar composi-

tions and microstructures, the latter consisting of plate-shaped grains with widths 1–2 μm and lengths 5–7 μm . However, their crack paths observed in the SEM were dramatically different. Y0.7 exhibited more than 80% intergranular fracture with multiple branching cracks, whereas Y0.5 exhibited $\sim 75\%$ transgranular fracture and almost no crack branching (see Fig. 1, insets). This change in fracture mode was reflected in the mechanical properties, in that both the strength and toughness were markedly higher in the Y0.7 material. Specifically, unnotched bending strengths were 25% higher with Weibull moduli a factor of two higher in Y0.7: bending strengths and Weibull moduli (in parenthesis) for Y.07 and Y.05 were 541 MPa (20.7) and 433 MPa (9.2), respectively. Average indentation toughness values (measured using $\sim 100 \mu\text{m}$ cracks), were over 40% higher for Y0.7 ($K_c \approx 5.5 \pm 1 \text{ MPa m}^{1/2}$), compared with Y0.5 ($K_c \approx 3.9 \pm 1 \text{ MPa m}^{1/2}$); similarly, using controlled-flaw bending tests, estimated toughness values were 53% higher in Y0.7 ($K_c \approx 4.9 \text{ MPa m}^{1/2}$) compared with Y0.5 ($K_c \approx 3.2 \text{ MPa m}^{1/2}$). Room temperature crack initiation values measured using the compact-tension specimens were 2.5 and 1.9 $\text{MPa m}^{1/2}$ for Y0.7 and Y0.5, respectively. High-temperature toughness measurements involving R-curve experiments at 1200 °C (Fig. 1) show an even larger difference in initiation toughness, i.e., 3.6 $\text{MPa m}^{1/2}$ in Y0.7 vs. 1.6 $\text{MPa m}^{1/2}$ in Y0.5, with a 70% higher steady-state (“plateau”) toughness value for the Y0.7 material. By comparison, 3ABC–SiC without RE additives has a room temperature toughness of 5.5 $\text{MPa m}^{1/2}$ [14], and RE-doped Si_3N_4 has a toughness of 2–4 $\text{MPa m}^{1/2}$ [3], both measured by the controlled-flaw method with a $\sim 100\text{-}\mu\text{m}$ critical crack size.

TEM examination of the crack paths in the vicinity of the grain boundaries revealed that the intergranular por-

tions of cracks followed one interface of the grain-boundary phase (GBP) material, as reported previously [4]. However, of particular note is that the GBP in the higher toughness Y0.7 material did not contain measurable amounts of Y. Fig. 2 shows representative nanoprobe-EDS scans of the crack faces in each material. The GBP in the Y0.5 ceramic is highly enriched in Al, O and Y; however, the Y0.7 material shows only heavy enrichment of Si and O and a minor amount of Al.

The absence of yttrium in the GBP in the higher toughness Y0.7 material was confirmed by HAADF-STEM imaging of intact grain boundaries: the intensity of HAADF-STEM images is proportional to the n th power Z^n ($n = 1.5\text{--}2$) of the average atomic number Z of the material being observed (these are therefore often referred to as Z -contrast images) [20,21]. Z -contrast images of the grain-boundary regions did not show differential contrast between the SiC grain and the boundary phase, indicating an approximately equal mass density in both regions (Fig. 3a). Z -contrast images of similar regions in the Y0.5 material show bright contrast along the grain boundary, indicating the presence of Y atoms (Fig. 3b).

Quantitative EDS was performed to estimate the Y content of the grain-boundary triple-point phases. In the Y0.5 material, these triple pockets were of approximately the same composition as the GBP, i.e., Al_2O_3 24 wt.%; Y_2O_3 15 wt.%; SiO_2 61 wt.%. In contrast, in the Y0.7 material, the composition of the triple pockets was Al_2O_3 48 wt.%, Y_2O_3 27 wt.%, SiO_2 25 wt.%, but the GBP was predominantly SiO_2 (Fig. 2). Indeed, while no mass contrast was visible at the grain boundaries in the Y0.7 material, the boundaries between SiC and triple pockets were decorated with Y (Fig. 3c).

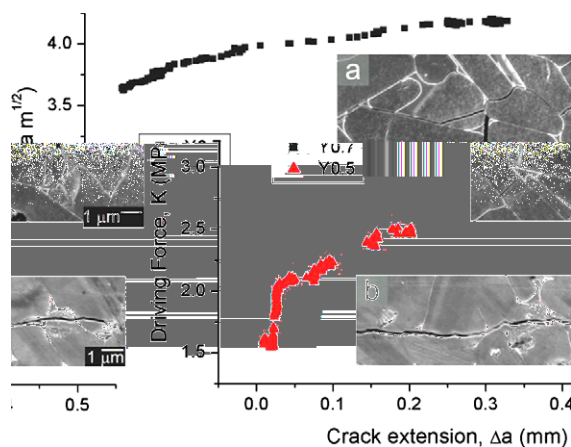


Fig. 1. Crack-growth R-curves measured in an argon atmosphere at 1200 °C for Y0.7 and Y0.5 SiC material. Rising R-curves are seen for both materials; however, the Y0.5 material has a universally lower toughness value. The steady-state (“plateau”) toughness of the Y0.7 ceramic, which fails intergranularly, is $\sim 70\%$ higher than that of the Y0.5 material, which fails transgranularly. Insets are crack paths in the: (a) Y0.7 and (b) Y0.5 ceramics. The Y0.5 material displays a nominally linear, transgranular crack path, whereas the higher toughness Y0.7 material shows extensive crack deflection and cracking along grain boundaries.

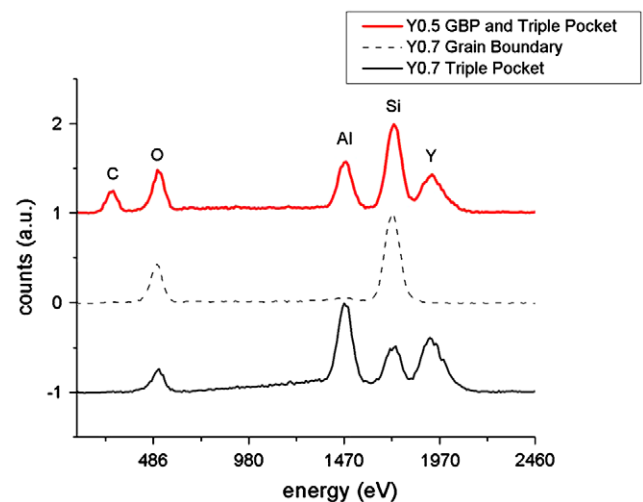


Fig. 2. Nanoprobe-EDS spectra of GBP containing crack faces and triple pockets in the Y0.5 and Y0.7 SiC microstructures. Y is clearly absent from the GBP in the Y0.7 material (center spectrum), but present in the triple pockets (bottom spectrum). The carbon peak is attenuated in the Y0.7 signal due to a greater sample thickness. By comparing the relative peak heights of Al, Si and Y with the EDS spectrum from Y0.5 (top spectrum), it is clear that Y ions in Y0.7 are collected in the triple pockets.

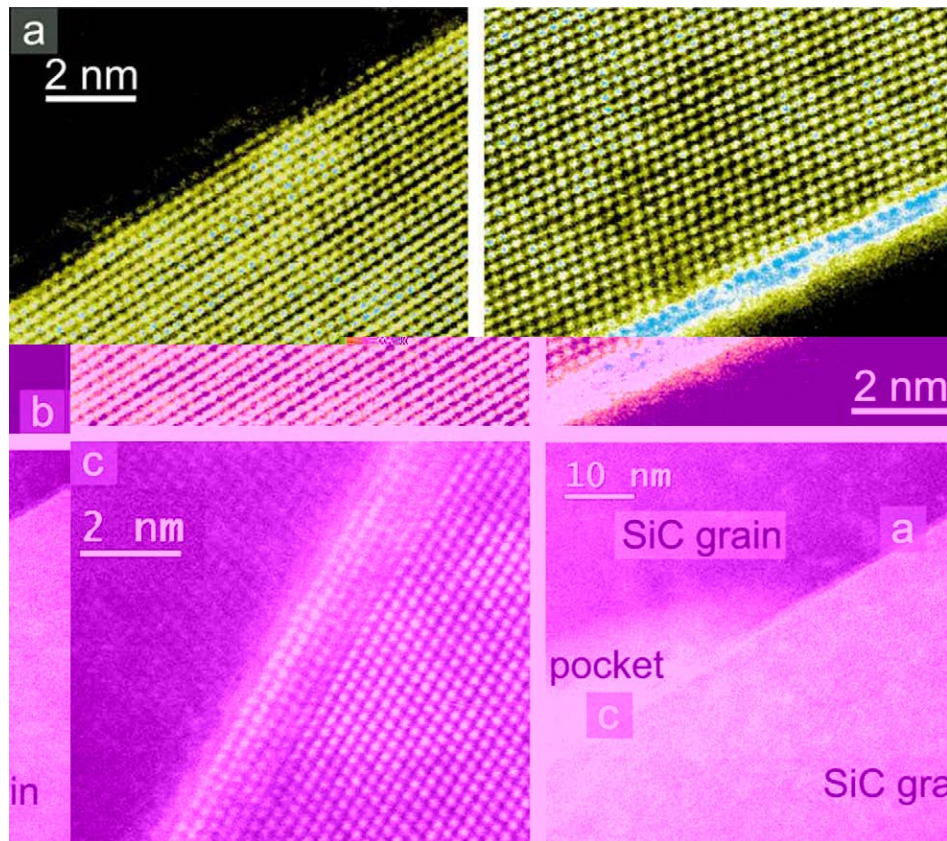


Fig. 3. Z-contrast STEM images of grain boundaries in: (a) Y0.7 and (b) Y0.5 silicon carbide materials. Color is tied to intensity and therefore mass; solid blue columns represent high mass Y ions. For the Y0.7 material in (a), no contrast is seen between the SiC grain and the GBP, indicating the absence of Y in the boundary phase. For the Y0.5 material in (b), bright contrast in the boundary phase indicates the presence of Y ions. (c) Z-contrast STEM image of a boundary between SiC (right) and a crystalline triple pocket (left) in the Y0.7 SiC material. The bright layer at the edge of the triple pocket is on average 40% brighter than the SiC lattice, indicating that it contains Y ions. The overview image on the bottom right shows the relative locations of images (a) and (c); the bright region at the left is a triple pocket.

4. Discussion

Although extensive studies [1–3,5–9,12,13,22–25] have been performed on the effect of yttrium additions on the structure and properties of SiC and Si₃N₄ ceramics,² difficulties in detecting Y and its location, by either EELS or Z-contrast imaging, have obscured its precise role. High-toughness microstructures in these materials rely on two conditions: a microstructure of interlocking elongated grains and the deflection of cracks around these grains (to achieve an intergranular fracture mode and effective toughening from grain bridging). RE additions have been shown to lead to the formation of glassy GBP, and to affect grain shape greatly, with concurrent variations in toughness across the RE series. What has not been discussed in as much detail is the role of these RE additives in controlling crack deflection at the grain boundary, which represents the vital step in the development of an intergranular

fracture. Here, one sees that, given a nearly identical microstructure by using a single RE additive, the actual location of the Y ions within the microstructure at the atomic scale appears to be the key feature in determining the crack path, which in turn governs the fracture toughness at the macro-scale, evidence that microstructural control and the simple presence of an intergranular film are not solely sufficient to produce increased toughness.

Previous studies have shown that small changes in Y composition can influence the fracture behavior [2,8,9], although no clear explanation has been proposed. Furthermore, the final location of the Y dopants—within the GBP or solely in triple pockets and second phases—is sensitive to processing conditions, including the Y₂O₃:Al₂O₃:SiO₂ ratios and heat treatment. For example, it has been shown that the crystallization of YAG-type materials in triple pockets will remove Y from the GBP, leaving only Al, Si and O [13,22], although no previous correlation with fracture behavior had been made.

Computational studies by Painter et al. [23] corroborate these observations of varying segregation behavior. Y has been calculated to have approximately equal affinity for segregation to the grain surface (and therefore the grain boundary) or to collect in the triple pockets. This further

² While the Si₃N₄ field is rich in research on the nature of oxynitride glasses, similar research on the effects of RE doping is not available on oxycarbide glasses relevant to SiC. It is expected though that trends in physical properties such as elastic modulus in RE-doped SiAlON glasses/grain-boundary films will be similar in RE-SiAlOC glasses.

suggests that minor changes in processing, including temperature, pressure and chemistry, could stimulate a particular segregation behavior.

For the present Y-doped SiC, to understand why GBPs deficient in Y (in Y0.7) generate deflected cracks at grain boundaries and intergranular fracture, whereas the presence of Y in the GBP (in Y0.5) does not, one needs to examine the relative stiffness of these phases and how this affects crack deflection at the boundaries. Quantitative information, either experimental or computational, on the moduli of the GBP compositions observed here, however, is not available. An estimate of the moduli was made using a simple rule of mixtures based on the moduli of the component oxides.³ While such an estimate is far from quantitative, together with trends in other glass systems [24–33], it nevertheless may provide a reasonable “best guess” for estimating the modulus mismatch across the interface, which can be characterized by the first Dundurs’ parameter; for the SiC/GBP combination, this is defined in terms of their respective moduli E_{SiC} and E_{GBP} as $\alpha = (E_{\text{SiC}} - E_{\text{GBP}})/(E_{\text{SiC}} + E_{\text{GBP}})$. The estimated Young’s moduli and resulting α values are listed in Table 1.

Images of cracks at grain boundaries, generated by microhardness indents in the TEM foils, are shown in Fig. 1; the objective here is to determine whether impinging cracks penetrate the boundary, as seen in Y0.5, or deflect along the SiC/GBP interface, as seen in Y0.7 (Fig. 4). The tendency of a crack to penetrate through, or deflect along the GBP, may be considered in the context of the relative toughness of the SiC/GBP interface compared with that of the GBP, $G_{\text{Int}}/G_{\text{GBP}}$,⁴ together with the magnitude of the modulus mismatch α across the boundary, using the He and Hutchinson linear-elastic mechanics description of a crack impinging upon an elastic dissimilar material interface (Fig. 5) [4,34]. Depending upon the values of these parameters, incident cracks will either arrest and/or deflect along the interface (region I in Fig. 4) or penetrate it (region II). A major factor in determining the GBP modulus is the $\text{Y}_2\text{O}_3/\text{SiO}_2$ ratio. There is a significant difference in this ratio for the GBP, as is evident from the compositions superimposed on the $\text{Y}_2\text{O}_3\text{–SiO}_2\text{–Al}_2\text{O}_3$ ternary diagram (Fig. 6) [35], for Y0.5 and Y0.7. It should be noted that the alumina/yttria ratios of the triple pocket phases do not vary much for the two compositions examined, and that their alumina/yttria ratio after sintering is lower than expected on the basis of starting one. This is undoubtedly due to aluminum and alumina loss during the processing of alumina-containing SiC, which is a well-known phenomenon.

Crack deflection at the grain boundaries is essential for intergranular fracture to occur; without such a fracture mode crack-bridging mechanisms cannot develop, and the

Table 1

Measurements of the compositions of GBP and estimates of elastic modulus and first Dundurs’ parameter for Y0.5 and Y0.7, compared with SiC.

Sample	GBP composition Y_2O_3 ; Al_2O_3 ; SiO_2 (wt.%)	Estimated modulus, E (GPa)	Dundurs’ parameter α
Y0.5	15; 24; 61	115	0.59
Y0.7	Mainly SiO_2	186	0.73
SiC		450	

absence of such (extrinsic) toughness will not result in a rising R-curve and produce a minimal fracture toughness comparable with its intrinsic value, i.e., $\sim 2\text{–}3 \text{ MPa m}^{1/2}$ or less. The coupled observations of a change in the fracture mode—from intergranular to transgranular—with the inclusion of Y in the GBP shows that the increased modulus of such a Y-containing lower silica GBP (in Y0.5), compared with the Y-free, higher silica GBP (in Y0.7), can alter the path of a crack impinging on a boundary enough to change both the fracture behavior and the measured fracture toughness. Specifically, in Y0.5 material, the presence of Y ions in the boundary together with the lower SiO_2 content of the GBP leads to a stiffer GBP and hence to conditions where an incident crack will penetrate the SiC/GBP interface (Fig. 5), leading to transgranular fracture, no grain bridging, and corresponding poor toughness. With the absence of segregated Y in the boundaries and the higher SiO_2 content of the GBP in the Y0.7 material, the impinging crack will be deflected along the SiC/GBP interface as a result of the lowered modulus (i.e., higher α) of the GBP that it attempts to enter. The consequent deflection along the boundary leads to intergranular fracture, which in turn gives rise to grain bridging and superior fracture toughness (Fig. 5).

It is likely that processing conditions, particularly the (difficult to control) oxygen content and the sintering/heat treatment schedule, dictate the segregation behavior of Y-containing ABC–SiC, and therefore its fracture properties. While similar processing variables studied using this ABC–SiC system do not change the segregation behavior of RE ions such as La and Yb, the segregation of Y ions to the GBP is sensitive to both composition and thermal history.

For the low $\text{Y}_2\text{O}_3/\text{SiO}_2$ ratio GBP (Y0.7), a higher boundary stiffness should be expected from a simple estimate based on component moduli, as well from related work [23–28]. The low stiffness of the Y-free boundary phase can enhance crack deflection and increase toughness by changing the mechanical properties of the GBP [4]. The GBP of the Y0.7 material is primarily a silica-rich material, which should further decrease the stiffness of the boundary phase: for a $\text{SiO}_2\text{–SiC}$ boundary, the value of Dundurs’ parameter α would be ~ 0.73 , and crack deflection would be preferred even if the interfacial toughness approached that of the boundary phase itself. For this SiC ceramic doped with Y, crack-initiation fracture toughness values can be increased by up to 125% and R-curve plateau toughness values by 70% as a result of the separation of Y out of GBP or its interface. Additionally, it has been shown that

³ <http://www.ceramics.nist.gov/srd/summary/emodox00.htm>

⁴ G_i refers to the fracture toughness for phase “i” expressed in terms of the critical value of the strain-energy release rate. It is related to the (mode I) toughness expressed in terms of the stress intensity K by the expression: $G = K^2/E$, where E is Young’s modulus.

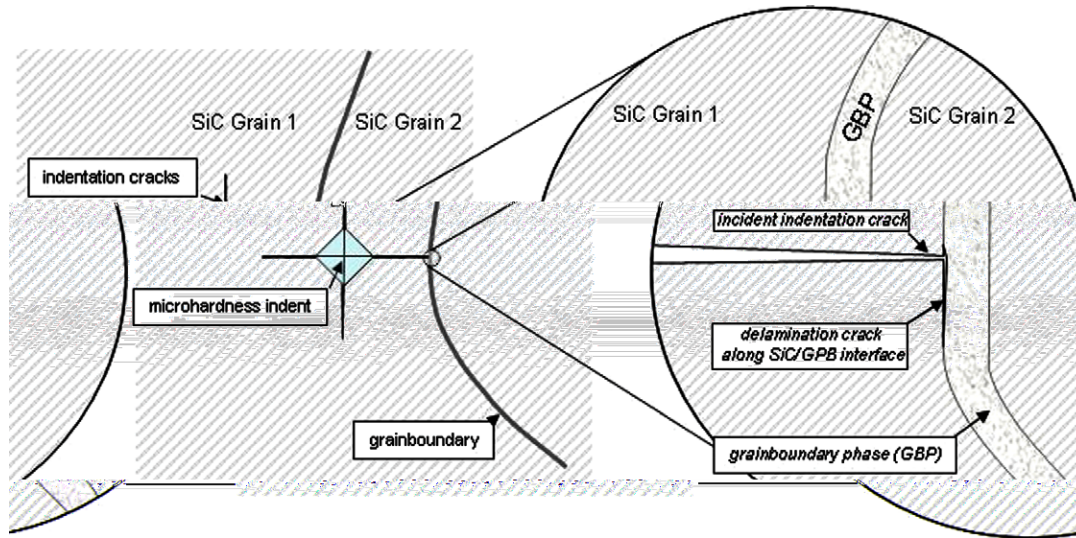


Fig. 4. Schematic representation of micro-indentation-produced cracks in the TEM foils impinging on a SiC grain boundary containing a grain-boundary phase (GBP) interaction. High toughness in the ceramic requires an intergranular fracture to generate toughening by grain bridging. This is only achieved when incidents crack deflect at the boundary, rather than penetrate it. This occurs in the Y0.7 material, but not in the Y0.5 material, by a process of “delamination” cracking at the first SiC/GBP interface.

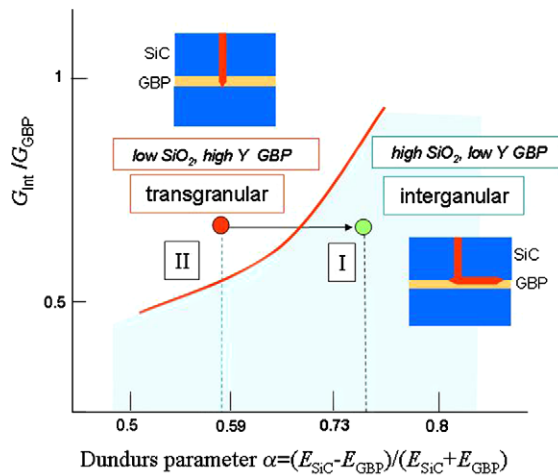


Fig. 5. He and Hutchinson model [34] linear-elastic mechanics solution for the case of a crack impinging normally on a dissimilar material interface. Whether the crack penetrates the interface or arrests/deflects along it depends on the elastic modulus mismatch across the interface, defined by the first Dundurs' parameter α , and the ratio of the interface toughness to that of the phase into which the crack attempts to propagate. In the present case of a crack propagating from the SiC matrix onto the GBP, $\alpha = (E_{\text{SiC}} - E_{\text{GBP}})/(E_{\text{SiC}} + E_{\text{GBP}})$, where E_i is the Young's modulus of phase i , and the toughness ratio is $G_{\text{Int}}/G_{\text{GBP}}$, where G_{Int} is the critical strain-energy release rate of the SiC/GBP interface, and G_{GBP} is the toughness of the grain-boundary phase. The curve on the plot marks the transition from crack deflection (region I) and crack penetration (region II). Crack deflection is essential to generate an intergranular fracture, a necessary event to ensure the occurrence of toughening by grain bridging and hence high fracture toughness. The Dundurs' parameters for the two different grain-boundary compositions are markedly different; accordingly, the relative modulus of the GBP with respect to the SiC is a significant factor in dictating the fracture behavior and hence the toughness of Y-doped ABC–SiC.

the crystalline Y-rich triple pockets that result from the removal of Y from the GBP can serve as anchors during

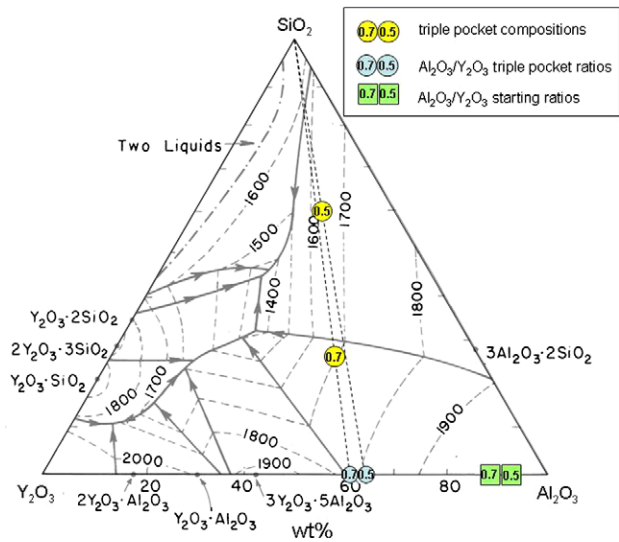


Fig. 6. Triple-point compositions and starting alumina/yttria ratios superimposed on ternary diagram for the $\text{SiO}_2\text{--Al}_2\text{O}_3\text{--Y}_2\text{O}_3$ system (compositions in wt.%) [35]. Note that the alumina/yttria ratio starting powder is higher than that found in the triple pockets after sintering. Y0.5 has a significantly higher SiO_2 content than Y0.7. The starting alumina/yttria ratio was set by the synthesis process, while the other compositions were determined from the EDS data (shown in Fig. 2).

high-temperature loading, decreasing grain-boundary sliding and improving creep resistance [13].

It is important to note that the action of the Y dopant is not to enhance toughness by “embrittling” the boundary phase, nor to reduce boundary failure by “strengthening” the boundary. The most significant effect is the increase in elastic modulus, which is separate from both the toughness and the strength of the phase. The change in modulus, compared with the fixed modulus of the SiC matrix, then alters crack deflection mechanics, as shown in Fig. 5.

Knowledge of the effects of sintering additives on the mechanical properties of the GBP, most importantly elastic modulus, can therefore drive the selection of dopants to achieve the desired fracture behavior.

5. Conclusions

With SiC doped with Y as an additive, processing variables such as yttrium and oxygen content and thermal history determine whether yttrium ions segregate to the GBP or are retained in the boundary triple pockets. This segregation behavior is primarily responsible for controlling the macroscopic fracture behavior through its influence on the elastic modulus of the GBP which controls whether incident cracks deflect or not at the SiC/GBP interface; such deflection leads to intergranular fracture, grain bridging and superior fracture toughness.

1. The presence of Y ions within the GBP in the SiC doped with 0.5 at.% Y correlates with a decreased SiO₂ content in the GPB which increases its stiffness; this decreases the likelihood of crack deflection at the boundary phase interface with the matrix due to the lower elastic mismatch across this interface. Such deflection is necessary for failure by intergranular cracking, which in turn is responsible for the primary toughening mechanism of grain bridging.
2. The lower stiffness of the GBP in the 0.7 at.% Y ceramic from the absence of Y in the boundaries and the higher SiO₂ content in the GBP, significantly increases the probability of such deflection, consistent with its much higher toughness.
3. While an elongated grain morphology is a necessary ingredient for toughened ceramics, intergranular fracture must be operative in order to utilize such beneficial microstructures to achieve high toughness. It is now clear that to develop Y-doped silicon carbide ceramics with reliably high toughness, the precise atomic location of the Y ions and the SiO₂ content must be understood and controlled.

Acknowledgements

This work was supported by the Director, Office of Science, Office of Basic Energy Sciences, Materials Sciences and Engineering Division, of the US Department of Energy under Contract No. DE-AC02-05CH11231. Part of this work was carried out using the facilities at the National Center for Electron Microscopy, which is supported at the Lawrence Berkeley National Laboratory by the Department of Energy under the same contract number.

References

- [1] Zhou Y, Hirao K, Toriyama M, Yamauchi Y, Kanzaki S. *J Am Ceram Soc* 2001;84:1642–4.
- [2] Satet RL, Hoffmann MJ, Cannon RM. *Mater Sci Eng A* 2006;422:66–76.
- [3] Becher PF, Painter GS, Shibata N, Waters SB, Lin H-T. *J Am Ceram Soc* 2008;91:2328–36.
- [4] Kueck AM, Kim DK, Ramasse QM, De Jonghe LC, Ritchie RO. *Nano Lett* 2008;8:2935–9.
- [5] Zhan G-D, Xie R-J, Mitomo M, Kim Y-W. *J Am Ceram Soc* 2001;84:945–50.
- [6] Rixecker G, Biswas K, Rosinus A, Sharma S, Wiedmann I, Aldinger FJ. *J Eur Ceram Soc* 2002;22:2669–75.
- [7] Gu H, Chen H, Guo L. *Mater Sci Eng A* 2008;491:177–81.
- [8] Winkelman GB, Dwyer C, Marsh C, Hudson TS, Nguyen-Manh D, Doblinger M, et al. *Mater Sci Eng A* 2006;422:77–84.
- [9] Kim J-Y, Kim Y-W, Mitomo M, Zhan G-D, Lee J-G. *J Am Ceram Soc* 1999;82:441–4.
- [10] Ritchie RO. *Int J Fract* 1999;100:55–83.
- [11] Kruzic JJ, Sadat RL, Hoffmann MJ, Cannon RM, Ritchie RO. *J Am Ceram Soc* 2008;91:1986–94.
- [12] Ziegler A, Kisielowski C, Hoffmann MJ, Ritchie RO. *J Am Ceram Soc* 2003;86:1777–85.
- [13] Gu H, Nagano T, Zhan G-D, Mitomo M, Wakai F. *J Am Ceram Soc* 2003;86:1753–60.
- [14] Cao JJ, MoberlyChan WJ, De Jonghe LC, Gilbert CJ, Ritchie RO. *J Am Ceram Soc* 1996;79:461–9.
- [15] Gilbert CJ, Cao J, MoberlyChan WJ, DeJonghe LC, Ritchie RO. *Acta Mater* 1996;44:3199–214.
- [16] Gilbert CJ, McNaney JM, Dauskardt RH, Ritchie RO. *J Test Eval* 1994;22:117–20.
- [17] Chen D, Gilbert CJ, Ritchie RO. *J Test Eval* 2000;28:236–41.
- [18] Sun EY, Becher PF, Hsueh C-H, Painter GS, Waters SB, Hwang SL, et al. *Acta Mater* 1999;47:2777–85.
- [19] Krivanek OL, Dellby N, Lupini AR. *Ultramicroscopy* 1999;78:1–11.
- [20] Hartel P, Rose H, Dinges C. *Ultramicroscopy* 1996;63:93–114.
- [21] Jesson D, Pennycook SJ. *Proc Roy Soc (London)* 1995;A449:273–93.
- [22] Zhan G-D, Ikuhara Y, Mitomo M, Xie R-J, Sakuma T, Mukherjee AK. *J Am Ceram Soc* 2002;85:430–6.
- [23] Painter GS, Becher PF, Shelton WA, Satet RL, Hoffmann MJ. *Phys Rev B* 2004;70:144108.
- [24] Chen J, Ouyang L, Rulis P, Misra A, Ching WY. *Phys Rev Lett* 2005;95:256103.
- [25] Ching WY, Chen J, Rulis P, Ouyang L, Misra A. *J Mater Sci* 2006;41:5061–7.
- [26] Lemerrier H, Rouxel T, Fargeot D, Besson J-L, Piriou B. *J Non-Cryst Solids* 1996;201:128–45.
- [27] Rouxel T, Huger M, Besson JL. *J Mater Sci* 1992;27:279–84.
- [28] Marchi J, Morais DS, Schneider J, Bressiani JC, Bressiani AHA. *J Non-Cryst Solids* 2005;351:863–8.
- [29] Rouxel T. *J Am Ceram Soc* 2007;90:3019–39.
- [30] Moysan C, Riedel R, Harshe R, Rouxel T, Augereau F. *J Eur Ceram Soc* 2007;27:397–403.
- [31] Walter S, Soraru GD, Brequel H, Enzo S. *J Eur Ceram Soc* 2002;22:2389–400.
- [32] Pantano CG, Singh AK, Zhang H. *J Sol-Gel Sci Technol* 1999;14:7–25.
- [33] Homeny J, Nelson GG, Paulik SW, Risbud SH. *J Am Ceram Soc* 1987;70:C114–6.
- [34] He M-Y, Hutchinson JW. *Int J Solids Struct* 1989;25:1053–67.
- [35] Bondar IA, Galakhov FYa. *Izv Akad Nauk SSSR, Ser Khim* 1963;7:1325 [reported as Fig. 2586 in Levin E, Robertins C, McMurdie H, editors. *Phase diagrams for ceramists*. Columbus (OH): American Ceramic Society; 1969].